# Oxygen distribution, incommensurate modulation, and structural disorder in $Bi_2Sr_2Ca_{1-y}Y_yCu_2O_{8+\delta}$ and $Bi_{10}Sr_{15}Fe_{10}O_{46}$ single crystals

T. Stoto and D. Pooke
*The New Zealand Institute for Industrial Research and Development, P.O. Box 31-310, Lower Hutt, New Zealand*

L. Forro
*Laboratoire de Physique des Solides Semi-cristallins, IGA, Ecole Polytechnique Fédérale de Lausanne, 1015 Lausanne, Switzerland*

K. Kishio
*Department of Superconductivity, Graduate School of Engineering, University of Tokyo, 7-3-1 Hongo, Bunkyo-ku, Tokyo 113, Japan*
(Received 20 November 1995; revised manuscript received 19 June 1996)

Electron diffraction and high-resolution electron microscopy along the *c* axis have been used to examine the local structural variations in modulated $Bi_2Sr_2Ca_{1-y}Y_yCu_2O_{8+\delta}$ and $Bi_{10}Sr_{15}Fe_{10}O_{46}$ single crystals in the as-prepared, underdoped, and overdoped state. In both materials the structural disorder, of which the structural modulation is one aspect, results from the labile nature of the BiO planes. A structural model for the BiO layers which explains the structural modulation and describes all the structural defects observed is suggested. A drastic change in the nature of the modulation due to an antiphase boundary structure appears in the highly substituted Y crystals in concomitance with the metal-insulator transition. The modified modulation contributes to the suppression of superconductivity by affecting the geometry of the CuO planes.
[S0163-1829(96)01345-8]

## I. INTRODUCTION

The high-temperature superconductor $Bi_2Sr_2CaCu_2O_{8+\delta}$ (Bi-2212) has an incommensurately modulated structure whose periodicity is 4.76 times the subcell lattice parameter *a*. The modulation has been attributed to the presence of extra oxygen in the BiO layers, reducing the mismatch between these planes and the perovskite blocks located between them.[1] The distortions induced by the modulation, its incommensurate character and the small x-ray and electron-scattering amplitudes of oxygen, compared to the heavy cations, complicate the refinement of the structure and the interpretation of high-resolution electron microscopy (HREM) images in terms of oxygen location.

Different space groups have been suggested for the average and modulated structures of Bi-2212, essentially falling into three categories. Several studies support the *A*-centered orthorhombic Bravais lattice, with the incommensurate component of the modulation wave vector parallel to the *a* axis, but with uncertainties remaining about the presence of a center of symmetry.[2,3] Second, many refinements have been performed using a primitive lattice[4–7] and a few investigations report electron- and x-ray-diffraction reflections incompatible with the *A*-type cell.[8,9] Third, other authors have suggested that the symmetry of the Bi-2212 phase is lower than orthorhombic.[10–12]

The attempts at determining the atomic positions of Bi and O, and in particular to locate the extra oxygen atoms, by single-crystal structural refinement have not given precise results apart from the confirmation of the presence of concentrated and diluted Bi regions.[13,14] The lack of information about the extra oxygen has contributed to the proliferation of structural models, which often are based on commensurate superstructures[4–7,12] or on the stacking of two types of supercells.[1,15,16]

The substitution of yttrium for calcium in Bi-2212 has been used to investigate the correlation between structural modulation and oxygen content. However the location of the extra oxygen, using x-ray-, neutron-, and electron-diffraction techniques, has been no more satisfactory than for the pure phase.[17–19] The principal characteristics of the structure do not change with increasing Y: the only variations concern the *c* parameter and the period of the incommensurate modulation which both follow a linear relationship with Y content.[20–22]

Apart from the disagreement over the exact location of the extra oxygen in the BiO layers and over the ''average symmetry'' of the structure, a further question is why the period of the modulation changes if the extra oxygen is inserted by cation substitution, but not by oxygen loading as evidenced in the pure phase.[23]

The study of the compound $Bi_{10}Sr_{15}Fe_{10}O_{46}$, isostructural with the Bi-2212 superconductor, but with a commensurate modulation of period five times the subcell period, has been more successful. The solution of this structure by Le Page *et al.* has allowed a more complete description of the oxygen distribution in the BiO layer based on the presence of two types of Bi-O arrangements: rocksalt-type and oxygen-deficient perovskite-type, corresponding to octahedral and square pyramidal oxygen coordination, respectively.[24]

The present study consists of a comparative characterization by electron diffraction and high-resolution electron microscopy of the structural disorder in $Bi_{10}Sr_{15}Fe_{10}O_{46}$ and in $Bi_2Sr_2Ca_{1-y}Y_yCu_2O_{8+\delta}$ single crystals in the as-prepared, underdoped, and overdoped states. Similarities and differences between the two kinds of compounds and in particular

 

between their structural defects have been related to the extra oxygen distribution in the BiO layers.

## II. EXPERIMENTAL DETAILS

$Bi_{10}Sr_{15}Fe_{10}O_{46}$ crystals were prepared using a method similar to that described by Le Page *et al.*[24] Approximately 10 g of source material of cation stoichiometry $Bi_3Sr_3Fe_2$ was prepared from $Bi_2O_3$, $SrCO_3$, and FeO, loaded into an alumina crucible, heated to 1250 °C, then cooled to 800 °C over a period of 105 h. Breaking the resulting mass apart, small flakes of material, translucent brown when thinly cleaved, were found and easily separated.

Single crystals of the $Bi_2Sr_2CaCu_2O_{8+\delta}$ (Bi-2212) phase were grown by the floating-zone technique in an infrared imaging furnace, using feed rods of cation stoichiometry $Bi_{2.1}Sr_{1.8}CaCu_2$.[25] The preparation of $Bi_2Sr_2Ca_{1-y}Y_yCu_2O_{8+\delta}$ single crystals is reported elsewhere.[20]

$Bi_{10}Sr_{15}Fe_{10}O_{46}$ and $Bi_2Sr_2CaCu_2O_{8+\delta}$ crystals were annealed at 765 °C in 0.2% oxygen in order to unload oxygen from the structure, while oxygen loading was attempted by annealing in 60 atmospheres of oxygen pressure with a slow cool from 500 to 350 °C, then holding at 350 °C for a period of two weeks. Other crystals were intercalated by sealing with elemental iodine in evacuated Pyrex-glass ampoules and annealing at 180 °C for periods of up to two weeks.

TEM foils were prepared by cleavage. Conventional transmission electron microscopy and energy dispersive spectroscopy microanalysis were performed at 100 keV, using a Philips EM400T microscope equipped with an energy dispersive x-ray analysis spectrometer. High-resolution observations were carried out at 300 keV, using the Philips EM430ST microscope of the Centre Interdépartemental de Microscopie Electronique, Ecole Polytechnique Fédérale de Lausanne, in Switzerland (point-to-point resolution 0.2 nm and spherical aberration constant 1.2 mm).

Calculations of electron-diffraction patterns, modeled supercells, and HREM images were carried out by using the software package EMS.[26] The software SEMPER (Ref. 27) was employed for Fourier filtration of the experimental images the details of which are described in the Appendix.

## III. RESULTS

### A. The structure of $Bi_{10}Sr_{15}Fe_{10}O_{46}$

The structure of $Bi_{10}Sr_{15}Fe_{10}O_{46}$ solved by Le Page *et al.*[24] is characterized by an orthorhombic unit cell with the fivefold modulation parallel to the $a$ axis ($a'=2.72$ nm$=5a$, $a=b=0.546$ nm, and $c=3.169$ nm) and the $B222$ space group. The sublattice period along the $a$ axis, $a=(1/5)a'$, and $b$ correspond to the $a$ and $b$ lattice parameters of the average unit cell of the isostructural cuprate, whereas $c$ is longer in the Fe compound because of the different composition of the perovskite blocks. Interplanar spacings and reflection conditions observed on the selected area electron-diffraction patterns of our single crystals confirm this structure.

Figure 1 illustrates different features of the structure of $Bi_{10}Sr_{15}Fe_{10}O_{46}$: the two kinds of Bi-O arrangements, described as rocksalt-type and bridging or oxygen-deficient perovskite-type by Le Page *et al.*,[24] the alternation along the $c$ axis of the positions of the extra oxygen lying at the center of the pseudoperovskite regions, the consequent distortions of the adjacent SrO-FeO-SrO-FeO-SrO blocks and the stacking of the BiO planes in the $B222$ structure. Note that sometimes the Bi atoms have been drawn using different sizes to differentiate $Bi^{3+}$ (ionic radius $\sim 1$ Å) from $Bi^{5+}$ (ionic radius$=0.74$ Å). The model of Le Page *et al.*[24] does not contain the $Bi^{5+}$ species, but from the ionic radii and bond lengths point of view their presence in the perovskite regions seems likely: a bridging oxygen is only 1.9 Å away from two Bi atoms. The perspective view of the BiO layers in the $B222$ structure of $Bi_{10}Sr_{15}Fe_{10}O_{46}$ shows clearly that Bi and O atoms are linked in ribbons running along the $a$ axis, perfectly superposed on each other, forming empty channels parallel to the $ac$ planes.

In order to understand the structural disorder of the Fe compound it is necessary first to be able to recognize on the high-resolution images the features typical of the perfect structure. Figure 2 shows the simulations of [001] zone axis high-resolution electron microscopy images corresponding to the different defocus values and the different crystal thicknesses exhibited by the experimental images of Fig. 3. Down the $c$ axis, the Bi atoms and the other cations form columns whose projection corresponds to the white dots on the 70 nm defocus images and to the black dots for 105 nm defocus. The dots corresponding to the rocksalt regions are elongated along **b**, the others, corresponding to the bridging regions, are more rounded. This kind of contrast does not change very much with the thickness. Because of the alternation of compressed and dilated regions along **c**, the periodicity of the modulation on the images is $2.5a$ instead of $5a$. The empty channels are visible on the HREM images as shown by the simulations. In fact, the contrast changes every second horizontal row of dots, i.e., every one-ribbon thick crystal slice parallel to the $c$ axis. This effect, which is even more evident if the images are looked at with a glancing angle, will be useful in the interpretation of the nature of the structural defects.

### B. Structural disorder in $Bi_{10}Sr_{15}Fe_{10}O_{46}$

All the crystals of $Bi_{10}Sr_{15}Fe_{10}O_{46}$ show some degree of imperfection. A synthesis of the structural defects observed by high-resolution electron microscopy and by selected area electron diffraction is displayed in Fig. 3.

Often the [001] zone axis diffraction patterns of the Fe compound are characterized by structural disorder of two forms: (1) rows of satellite spots due to the modulation, ($h\neq 10n$), slightly tilted with respect to the fundamental reflections ($h=10n$); (2) streaks along the rows of spots parallel to the $a^*$ direction with $k=2n+1$. Both defects, which are shown in Fig. 3(a), are related to translational disorder.

The tilt of the superlattice spot rows is an orientation anomaly and is typical of long period antiphase boundary structures containing periodic ledges or jogs, also called swinging planes, as shown by de Ridder, van Landuyt, and Amelinckx[28] and Van Tendeloo and Amelinckx.[29] In the case of the Fe compound the swinging planes are due to the fact that the pseudoperovskite regions in the BiO layers in adjacent unit cells are not aligned along the $b$ direction, but undergo a periodic shift of (1/2)**a**. Even if there is perfect

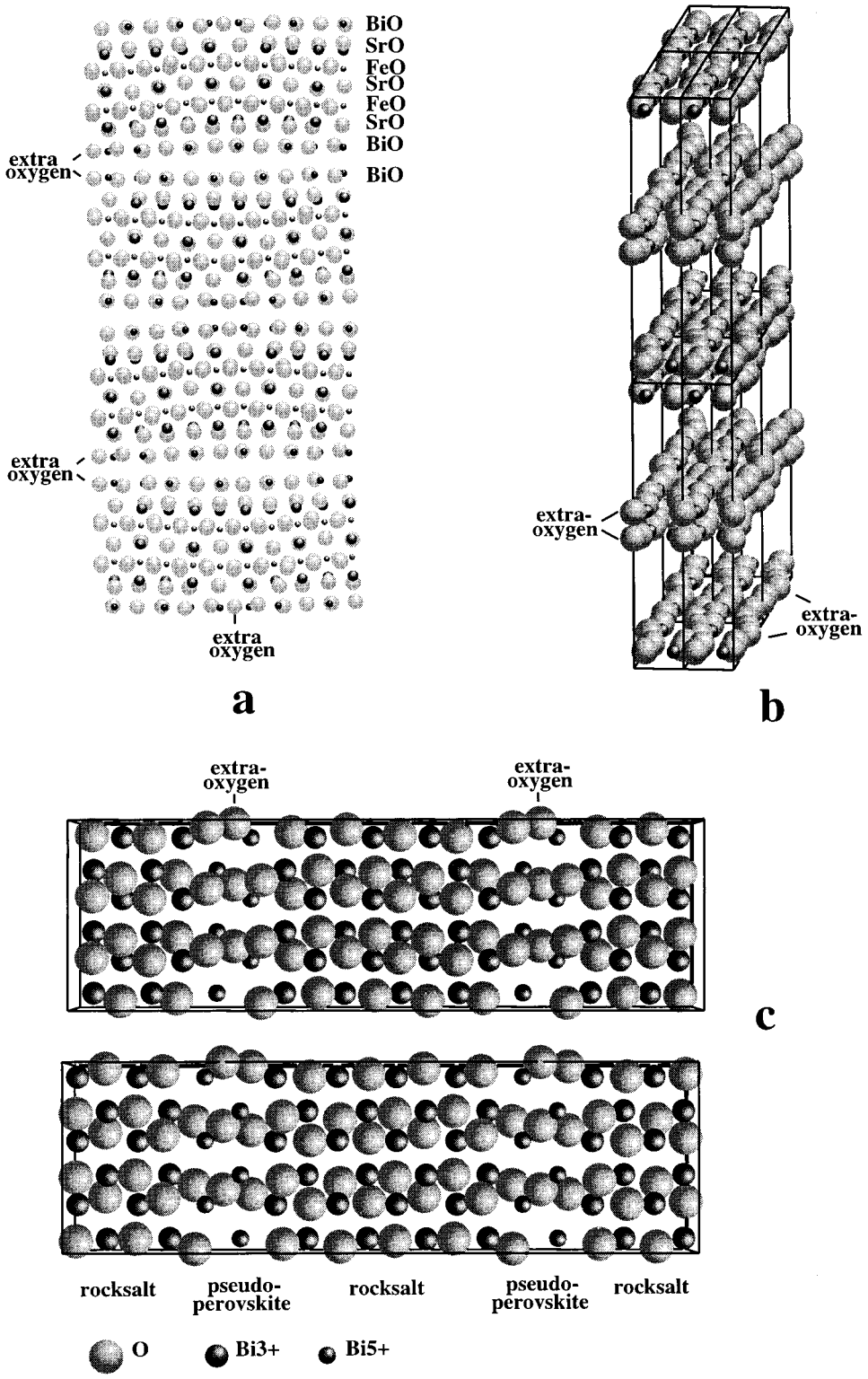


FIG. 1. (a) Projection [010] of the $Bi_{10}Sr_{15}Fe_{10}O_{46}$ showing the alternation of the position of the extra oxygen along the *c* axis, the contraction and expansion of rocksalt and bridging regions, respectively, and the consequent distortions of the adjacent perovskite blocks. (b) Perspective view of the structure of $Bi_{10}Sr_{15}Fe_{10}O_{46}$ without the perovskite blocks. The BiO double layers consist of BiO ribbons running along the *a* axis with the extra-oxygen atoms facing each other. (c) Projection down the *c* axis of the pair of adjacent BiO layers centered at $z=0$ showing the rocksalt-type and bridging (or oxygen-deficient perovskite-) type of Bi-O arrangements.

order along **a**, the direction of the satellite spots is not parallel to the modulation direction and hence the name orien--tation anomaly. In the schematical model of Fig. 3(b) there is a shift every second unit cell. A new periodicity arises because of the periodic character of the defect, and the orientation of the new supercell, called a ''shear block,'' determines the tilt of the spots in the diffraction pattern. This defect is very important from the point of view of the corre-

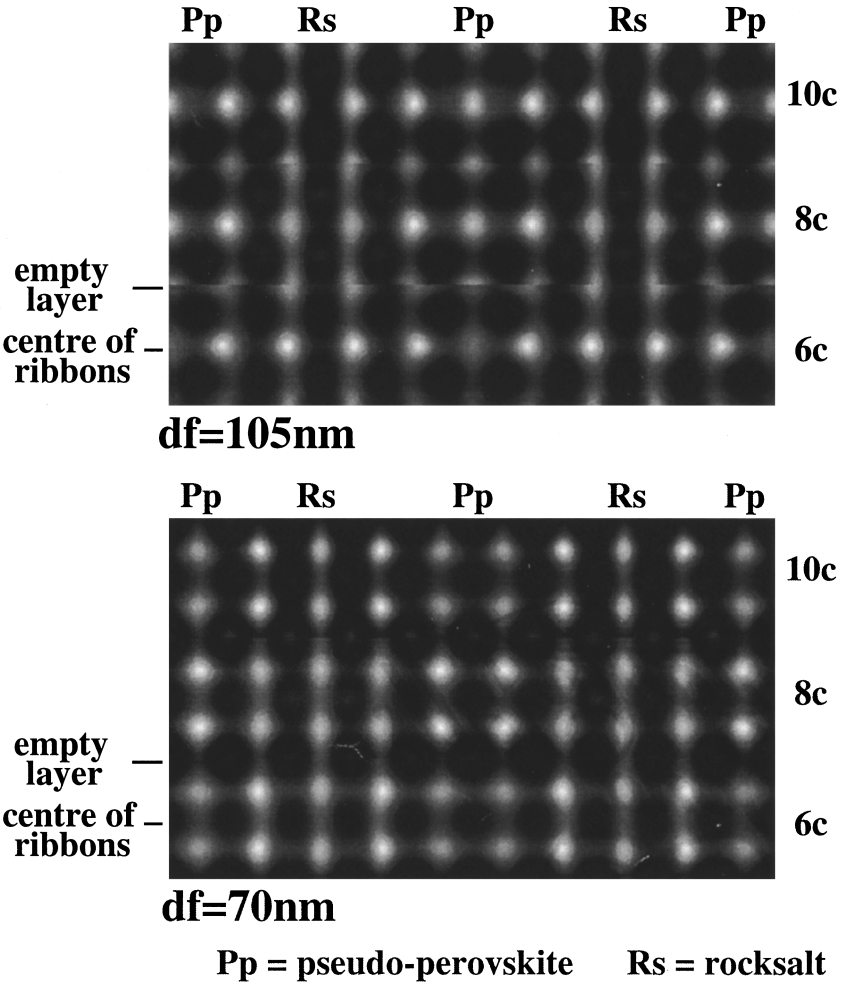


FIG. 2. Simulation of the [001] zone axis high-resolution images of $Bi_{10}Sr_{15}Fe_{10}O_{46}$, corresponding to one unit cell, two defocus values, and three different thicknesses.

lation between extra oxygen and the modulation. In fact the diffraction effect observed is strictly due to the distribution of extra oxygen atoms and confirms their role in determining the periodicity of the modulation.

The streaks along the rows of spots parallel to the $a^*$ direction with $k=2n+1$ are the manifestation of nonperiodic antiphase boundaries perpendicular to the $a$ axis characterized by a translation vector $\mathbf{R}=(1/2)[010]$ as indicated by the model of van Landuyt *et al.*[30] based on the kinematic theory of electron diffraction. A filtered HREM image containing this kind of defect is shown in Fig. 3(c): three domains are visible, the structural ribbons in the central domain are displayed by half a unit cell along **b** with respect to those in the lateral regions. The structural model suggested shows that this defect is due to a $(1/2)\mathbf{b}$ shift of the three bridging oxygen atoms in the pseudoperovskite regions of adjacent unit cells along **a**.

The contrast characteristic of the ribbons sometimes disappears as shown in Fig. 3(d), indicating that the empty channels of the structure are no longer aligned along the $c$ axis. There are two possible reasons. The first is the presence of antiphase boundaries perpendicular to **c** characterized by a translation $(1/2)\mathbf{b}$. The second is the existence, locally, of another kind of crystal symmetry with the BiO double bilayers stacked in alternated positions instead of perfectly superposed as with the $B222$ space group.

Another important defect contributing to the disorder of $Bi_{10}Sr_{15}Fe_{10}O_{46}$ is shown in Fig. 3(e). The processed HREM image shows that the periodicity of the modulation is not perfectly commensurate, with the distance between pseudoperovskite regions sometimes being $4.5a$ instead of $5a$. Rocksalt and perovskite regions are clearly visible on the image because of their different contribution to the contrast: the rocksalt regions correspond to the brightest regions as shown by the simulations in Fig. 2. The contrast shows that the ribbons are still perfectly aligned along **a**. The structural model shows that this faulted unit cell is due to a contraction $(1/2)a$ of the rocksalt region. This short unit cell creates extra disorder along **c**. In fact, the 4.5-fold periodicity cannot propagate along the $c$ axis because it is incompatible with the alternation of the positions of the extra oxygen: there is no perovskite site for the extra oxygen perfectly aligned with the center of the rocksalt regions belonging to the adjacent BiO double layers. The extra-oxygen atoms can choose the perovskite site slightly to the left or to the right, which are equivalent. Considering the distance between BiO bilayers no correlation can be expected between the position of the pseudoperovskite regions in the layers at the top and at the bottom of the faulted cells. This misalignment is the reason why on the high-resolution images the contrast due to the perovskite regions of the $4.5a$ supercell is less distinct.

To sum up, the structural disorder in $Bi_{10}Sr_{15}Fe_{10}O_{46}$ is related to the fact that in the perovskite regions of the BiO layer the oxygen atoms do not fully occupy all the sites available. The occupation of different kind of sites in adjacent unit cells along the three axes, induced by the transla-

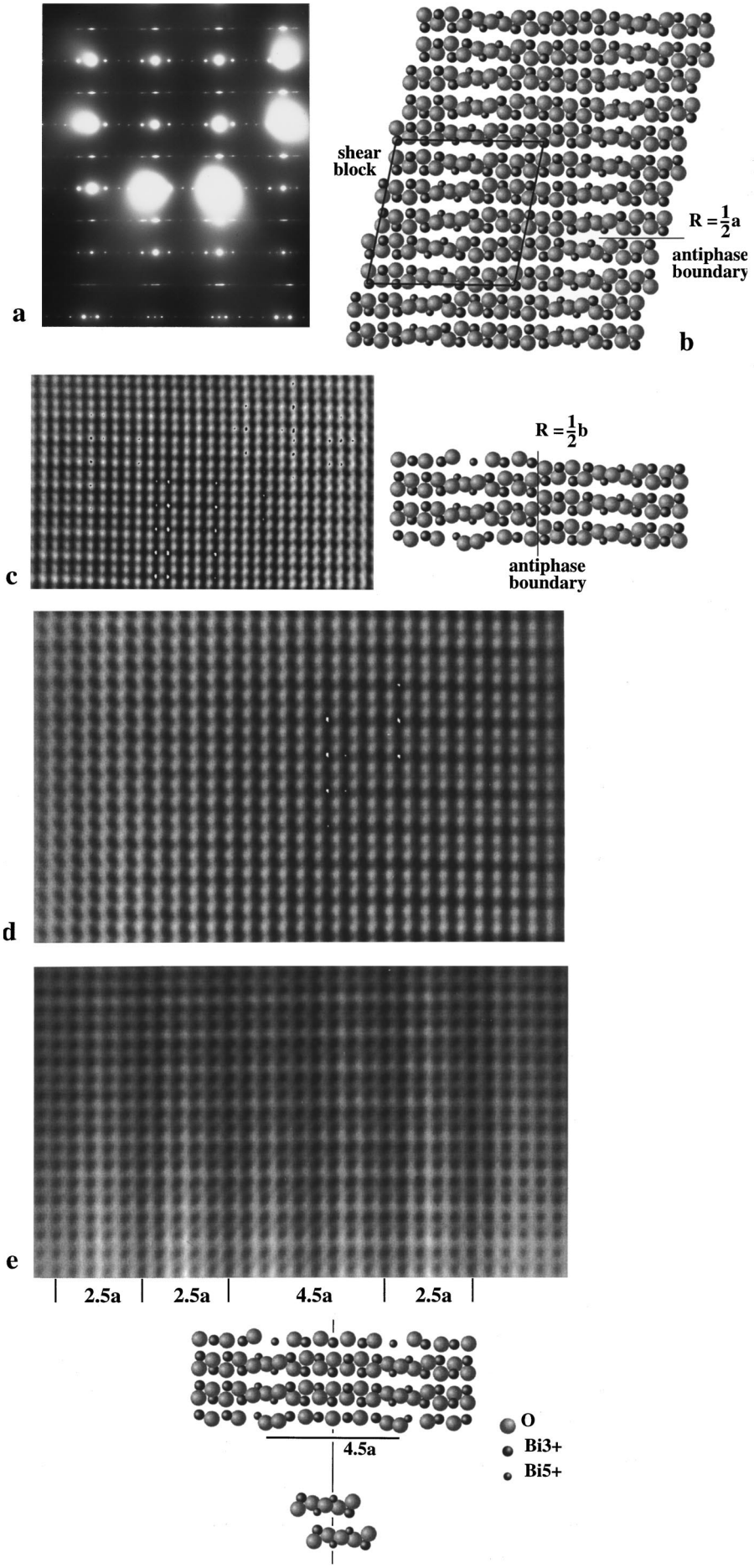


FIG. 3. (a) [001] zone axis diffraction patterns of the Fe compound showing two effects of the structural disorder: (1) an orientation anomaly, i.e., rows of satellite spots due to the modulation, $(h \neq 10n)$, slightly tilted with respect to the fundamental reflections $(h = 10n)$; (2) streaks along the rows of spots parallel to the $a^*$ direction with $k = 2n + 1$. (b) Schematical structural model showing the kind of long period antiphase boundary structure, based on swinging planes, that produces the tilt of the superlattice spot rows in the diffraction pattern. The ''shear block,'' whose orientation determines the tilt of the spots in the diffraction pattern is indicated. (c) [001] zone axis HREM image containing two antiphase boundaries perpendicular to the $a$ axis characterized by a translation vector $\mathbf{R} = (1/2)\,[010]$: three domains are visible, the structural ribbons in the central domain are displaced by half a unit cell along **b** with respect to those in the lateral regions. The structural model suggested shows that this defect is due to the shift $(1/2)\mathbf{b}$ of the three bridging oxygen atoms in the pseudoperovskite regions in adjacent unit cells along the $a$ direction. (d) [001] zone axis HREM image showing that the typical contrast due to the ribbons present in the right side disappears in the left side, indicating that the empty channels of the structure are no longer aligned along the $c$ axis. (e) [001] zone axis HREM image showing a faulted 4.5-fold unit cell. The structural model shows that this faulted unit cell is due to a contraction $(1/2)a$ of the rocksalt region. The 4.5-fold periodicity cannot propagate along the $c$ direction: the two possible configurations of the extra oxygen in the adjacent BiO double layers are indicated.

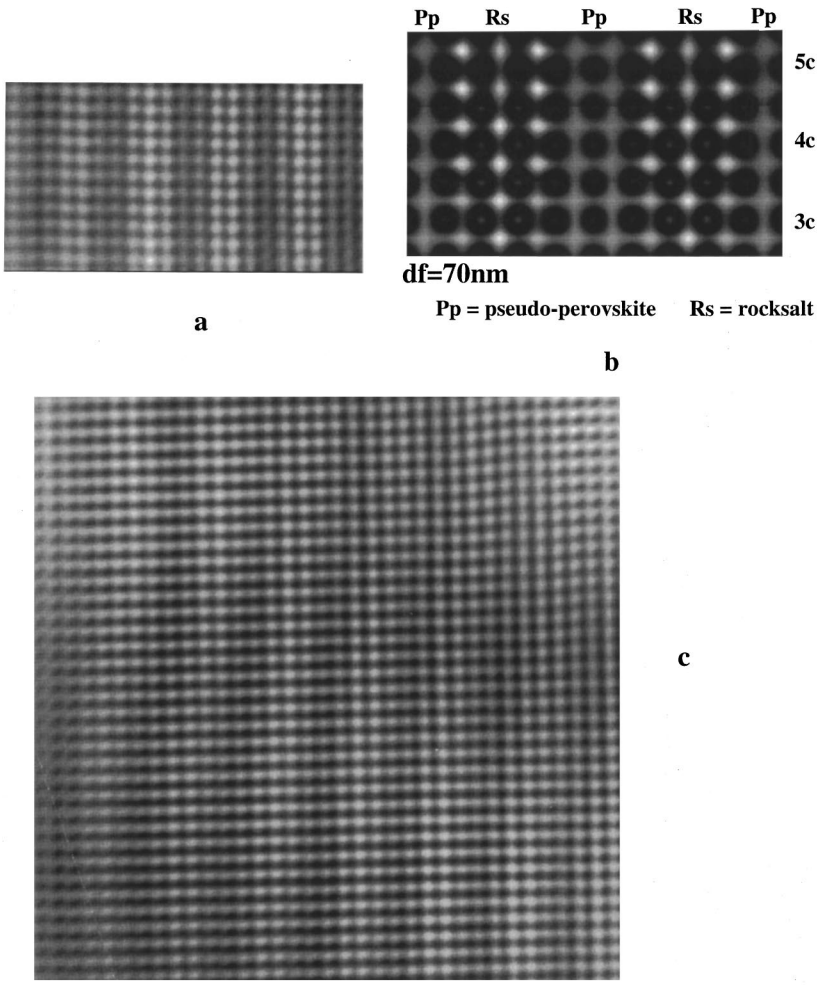


FIG. 4. (a) HREM image corresponding to the projection down the *c* axis of the pure Bi-2212 compound showing that the incommensurate character of the modulation is due to the stacking along **a** of three supercells with different sizes along the *a* axis. (b) Simulations of the HREM images along the [001] zone axis using a structural model developed from that of the Fe compound. (c) [001] zone axis HREM image showing swinging planes due to the fact that the pseudoperovskite regions in the BiO layers in adjacent unit cells are not aligned along the *b* direction, but they are shifted (1/2)**a**.

tions (1/2)**a** and (1/2)**b**, with or without contraction of the rocksalt region in between, is the mechanism behind all the defects observed.

### C. The structure of $Bi_2Sr_2Ca_1Cu_2O_{8+\delta}$

Selected area electron-diffraction patterns and HREM images corresponding to the projection down the *c* axis of the pure Bi-2212 compound have been compared to those of the Fe compound. Although in our previous work the modulation direction has been chosen along the *b* axis, here we prefer to consider it along the *a* axis for comparison with the Fe compound.[20] The main differences between the two compounds are the incommensurate character of the modulation due to the stacking along **a** of supercells of different size and the absence of any indication of empty channels between ribbons as shown in Fig. 4(a). This does not mean that in the cuprate Bi and O atoms are not linked in a ribbon configuration, but only that in adjacent BiO double sheets they are stacked in alternated positions preventing the formation of the empty channels [Fig. 5(a)]. This kind of stacking is clearly visible on the HREM images of Matsui *et al.*[31] corresponding to the projection down the direction of the modulation.

Simulations of the HREM images along the [001] zone axis using a variety of structural models based on extra oxygen atoms occupying different perovskite sites[5,7,32] and a model based on the displacive modulation of the Bi atoms without extra oxygen[4] have not shown agreement with the observed images. On the other hand, the images calculated from a structural model developed from that of the Fe compound, after requisite modifications accounting for the different stacking of the BiO ribbons along **c**, reproduce the experimental contrast satisfactorily, as shown in Fig. 4(b). This model is based on BiO layers containing oxygen-deficient perovskite regions, 1.5*a* wide as in $Bi_{10}Sr_{15}Fe_{10}O_{46}$, and spaced by rocksalt regions of varying widths. The three basic supercells, whose extent along the *a* axis are 5*a*, 4.5*a*, and 4*a*, respectively, are shown in Fig. 5(b). For thicknesses up to about 20 nm, i.e., 6–7 unit cells, the distribution of the different supercells is quite uniform along **c** and leads to the formation of blocks containing only four- or only fivefold supercells. Due to their different contribution to the contrast, perovskite and rocksalt regions are easily recognizable on the images: the rocksalt regions are brighter. Note that, as in the case of the Fe compound, the periodicity of the modulation on the images is half the real one because of the alternation between rocksalt and pseudoperovskite regions along **c**. The width of rocksalt regions is variable, whereas that of pseudoperovskite ones does not change. The contrast corresponding to the 4.5*a* supercell is slightly different because the 4.5*a* periodicity cannot expand along the *c* axis, as already mentioned. The indication that the size of pseudoperovskite regions is constant is very important because it means that there are always linear arrangements of three

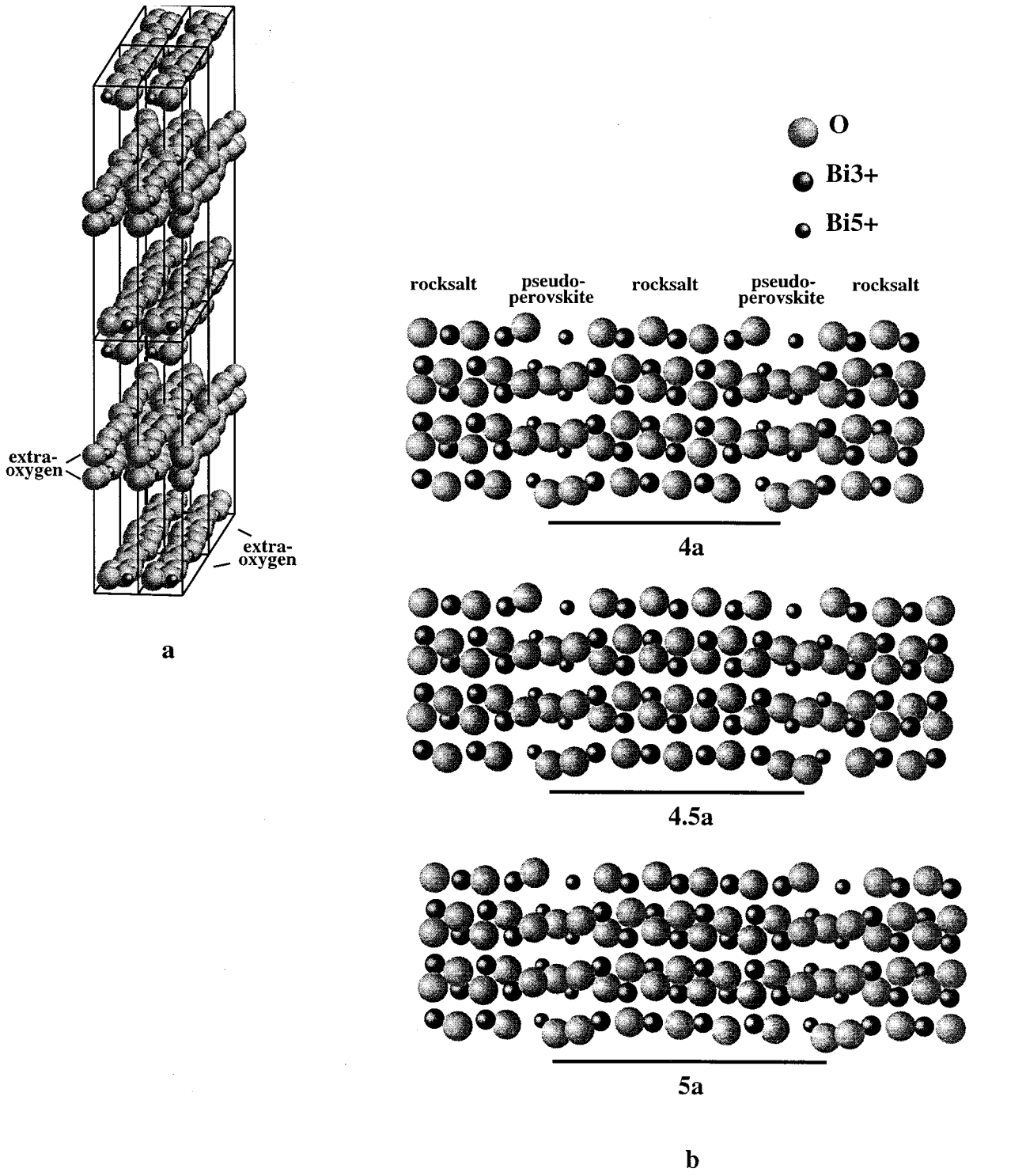


FIG. 5. (a) Perspective view of the structure of the pure phase Bi-2212 without the perovskite blocks. The position of the BiO ribbons belonging to adjacent BiO bilayers is alternated, preventing the formation of empty channels. (b) Schematical models of the three basic BiO supercells, whose size along the $a$ axis are $5a$, $4.5a$, and $4a$. There are always linear arrangements of three bridging oxygen atoms occupying three out of the six available perovskite sites as in the Fe compound.

bridging oxygen atoms occupying three out of the six available perovskite sites, exactly as in the Fe compound. This is also the main reason for the disagreement between simulations from previously proposed models and observed images: the contrast of their perovskite regions is unlike the experimental one because of the different number and/or location of the bridging oxygen atoms.[5,7,32]

Our model is based on a primitive lattice. The calculations involving the five and four supercells have been performed using the $Pnnn$ space group. Any $A$-centered orthorhombic Bravais lattice is incompatible with our observations because it does not describe the alternation of the positions of the extra oxygen atoms, and hence of rocksalt and pseudoperovskite regions, along **c**.

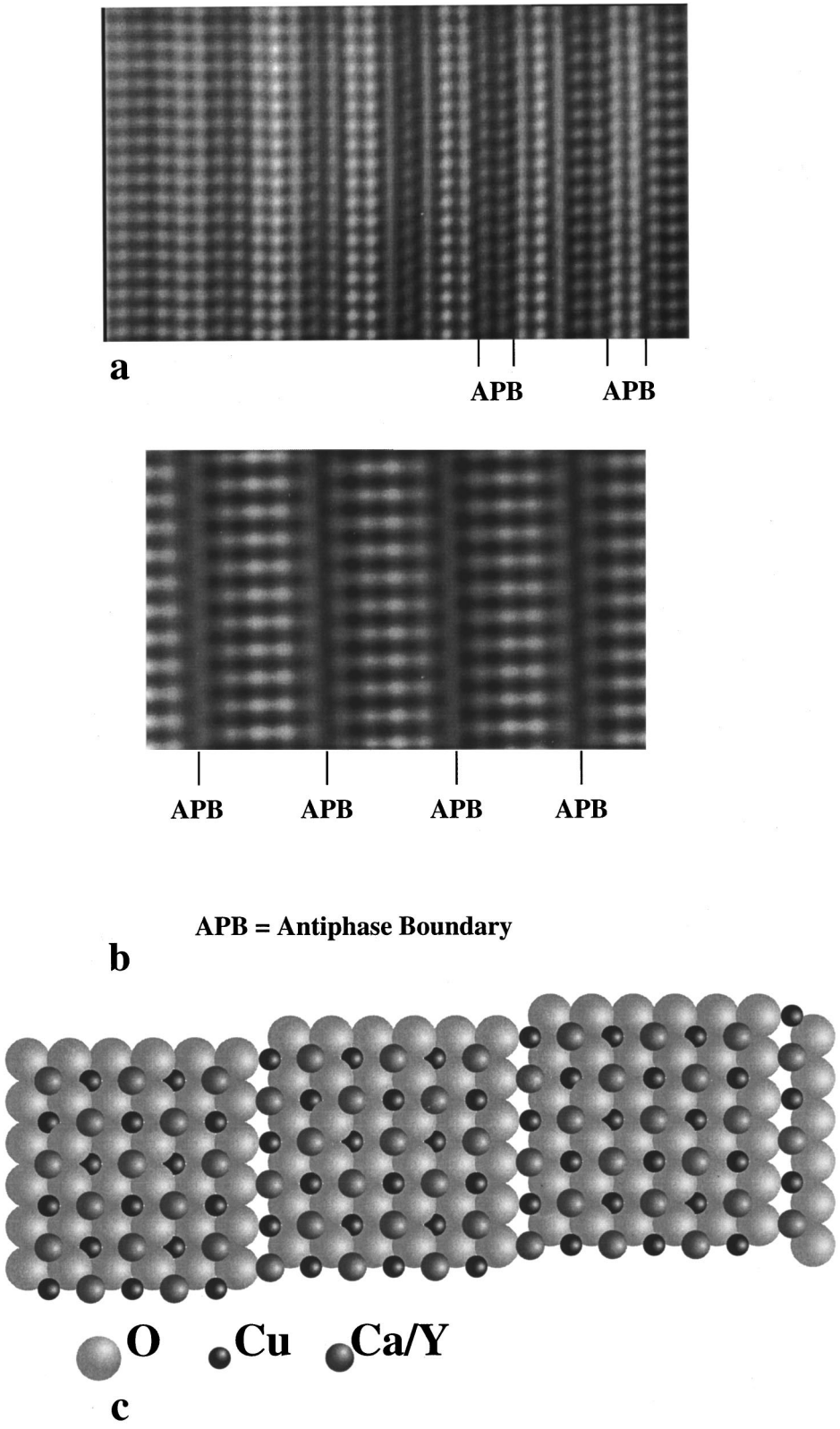


FIG. 6. (a,b) HREM images of the crystal structures of Y-substituted Bi-2212 single crystals with low (a) and high (b) yttrium content in the projection down the *c* axis. The structure of the low Y crystals is very similar to that of the pure phase despite a stronger disorder along **c** indicated by the merging of dots in lines (a). With increasing Y content an antiphase domain structure appears: the translation interfaces perpendicular to the *a* axis and corresponding to a translation vector (1/4)[010] are indicated (b). A few antiphase boundaries are already present in very weakly substituted crystals at the boundaries between rocksalt and pseudoperovskite regions as indicated (a). (c) Schematic representation of the domain structure of the $CuO_2$ planes of Y-rich Bi-2212 crystals due to the presence of translation interfaces.

### D. Structural disorder in $Bi_2Sr_2Ca_1Cu_2O_{8+\delta}$

As a consequence of their very similar BiO sublattice, the structural disorder in Bi-2212 and $Bi_{10}Sr_{15}Fe_{10}O_{46}$ has the same nature. In addition to the 4.5*a* supercell present in both compounds the HREM observations of the projection down the *c* axis have shown the existence of swinging planes [Fig. 4(c)]. This defect, which is responsible for the disorder along **b**, is even more complex in the cuprate because it can also be created by the stacking along the *b* direction of cells with different periods. We have not observed diffraction effects due to periodic jogging in our single crystals, but only localized defects on the lattice images. However, orientation anomalies have already been observed in single crystals of Bi-2212.[2,22,33] Goodman *et al.*[2] have considered the exist-

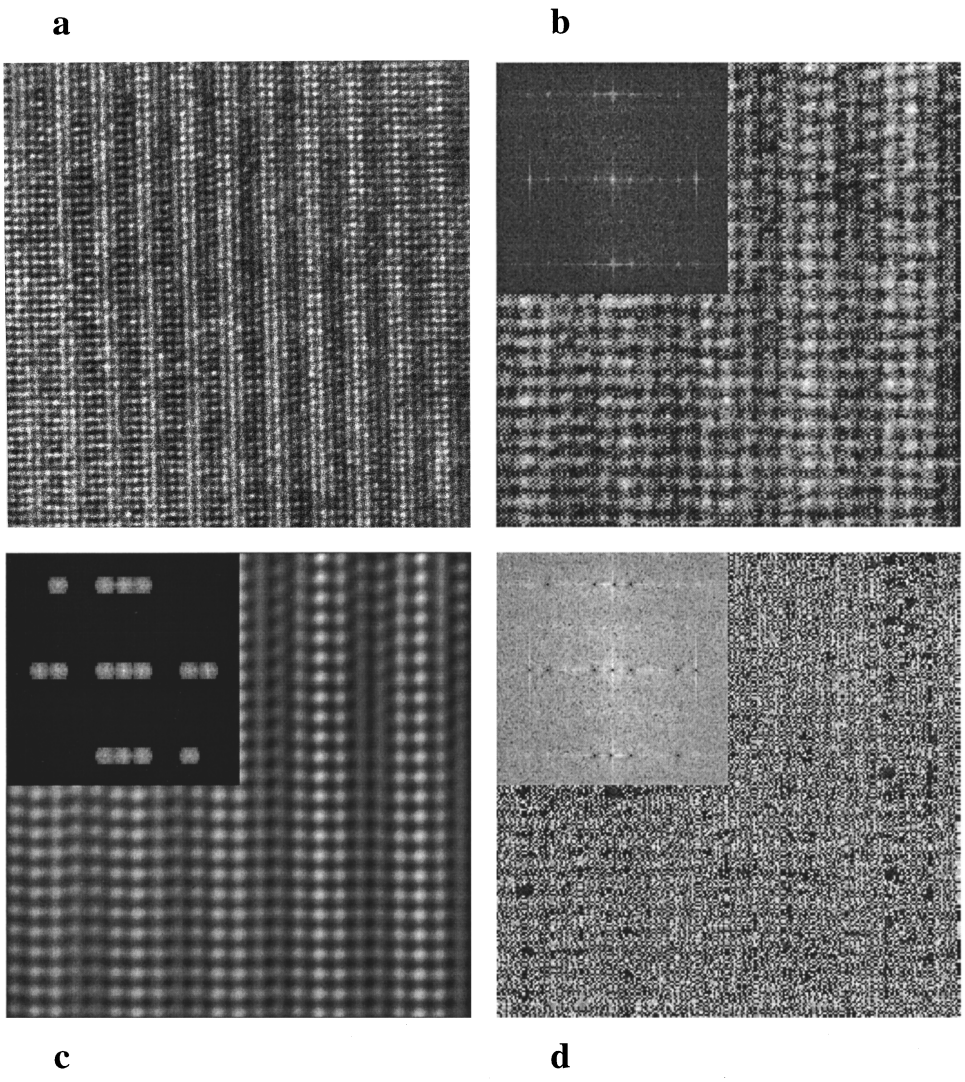


FIG. 7. (a) HREM image of a Y-substituted Bi-2212 single crystal with low yttrium content before noise filtering. (b) Histogram-equalized image extracted from the raw micrograph with the corresponding power spectra (log display). (c) Images reconstructed by inverse transformation from a soft Gaussian mask with the corresponding power spectra. (d) Image reconstructed by inverse transformation from the complementary mask with the corresponding power spectra.

ence of an unidentified ''swinging'' crystallographic shear plane structure, whereas other authors have wrongly attributed them to a possible small $b^*$ component of the incommensurate modulation.[22,33]

The disorder along **c** is stronger in the cuprate because of the more frequent occurrence of 4.5*a* supercells and also because of stacking of supercells with different periods. Intense x-ray streaking along the *c* axis, indicating disorder in this direction, has been observed by Kan *et al.*[33] Since in the cuprate the BiO ribbon stacking along **c** prevents the formation of empty channels, the antiphase boundaries perpendicular to the *a* and the *c* axes, characterized by the translation (1/2)**b**, observed in the $Bi_{10}Sr_{15}Fe_{10}O_{46}$ single crystals are not detectable in the [001] orientation. However, the observations of Budin *et al.* along the direction of the modulation show clearly that this kind of translation exists and it is responsible for the formation of a different structure which corresponds exactly to the *B*222 symmetry of the Fe compound.[8] This also indicates that the description of the Bi-2212 structure on the basis of a particular space group is not appropriate because the local symmetry is very variable depending on the relative positions of the extra oxygen atoms in two adjacent unit cells along the three axes.

The incommensurate character of the modulation is the consequence of the tridimensional structural disorder in the BiO layers. In 1957, Fujiwara showed that sharp superstructure reflections corresponding to noninteger *M* in the diffraction patterns could be given by a statistical distribution of integral *m* domains distributed such that over any reasonably large distance the average domain size corresponds to the nonintegral *M* value.[34] In the case of Bi-2212, *M* is 4.76*a* and corresponds to the average distance, along the *a* direction, between the extra oxygen atoms at the center of the pseudoperovskite regions in the BiO planes.

### E. Extra oxygen due to annealing under high oxygen pressure

Despite the high oxygen pressure (60 atm) used during annealing, the period of the structural modulation on the diffraction patterns of the Bi-2212 cuprate does not change. The same behavior occurs in the Fe compound. Further oxygen loading has no effect on the HREM images corresponding to the [001] zone axis of the two compounds. This is consistent with the unchanged modulation and indicates that the rocksalt-pseudoperovskite structure of the BiO layers is not altered during oxygen loading and unloading. However, in both materials it is possible to follow the introduction of extra oxygen because the *c* parameter decreases with increasing the oxygen content. In the case of $Bi_{10}Sr_{15}Fe_{10}O_{46}$ single crystals in the as-prepared state, x-ray diffraction

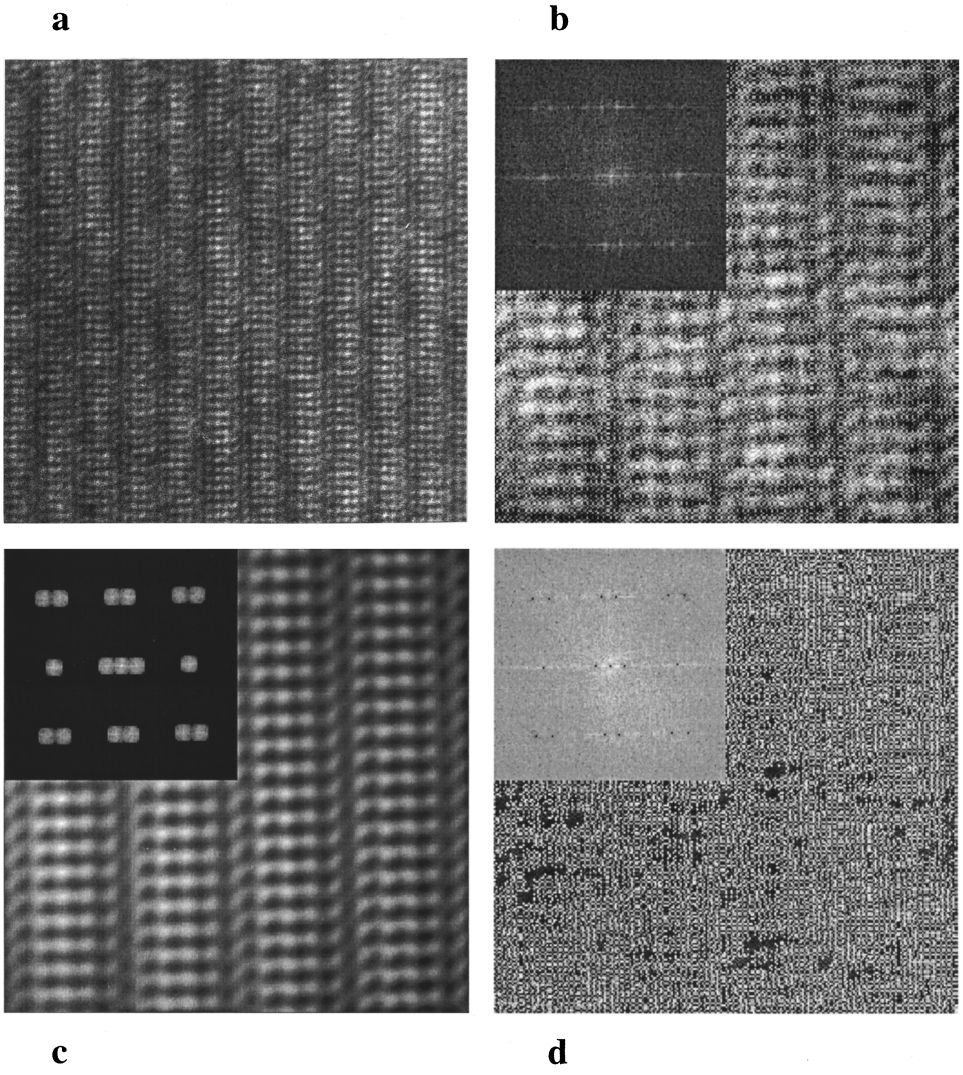


FIG. 8. (a) HREM image of a Y-substituted Bi-2212 single crystal with high yttrium content before noise filtering. (b) Histogram-equalized image extracted from the raw micrograph with the corresponding power spectra (log display). (c) Images reconstructed by inverse transformation from a soft Gaussian mask with the corresponding power spectra. (d) Image reconstructed by inverse transformation from the complementary mask with the corresponding power spectra.

yielded a $c$ parameter of 3.151 nm, rising to 3.17 nm in the unloaded state, and compressing to 3.144 nm in the oxygen-loaded state. The same trend has been observed in the cuprate: the $c$ parameter was 3.074 nm after oxygen loading and 3.09 nm in the unloaded state.

The period of the modulation seems related to the optimal stoichiometry, $\delta=0.21$, via an excess of 0.105 oxygen atoms per Bi. Using our model, this situation corresponds to about 19 Bi atoms surrounded by 15 oxygen atoms in the rocksalt positions and six in the pseudoperovskite linear arrangements over the 12 available sites. We have not measured the oxygen content of our crystals, but the study of Mitzi *et al.*[23] of $Bi_{2.1}Sr_{1.94}Ca_{0.88}Cu_{2.07}O_{8+\delta}$ single crystals has shown that the maximum uptake is 0.29 oxygen atoms per formula unit corresponding to a shortening of 0.009 nm of the $c$ parameter. This means a further excess of 0.04 oxygen atoms per Bi with respect to the optimal stoichiometry. Since neither the structure nor the structural modulation change because of these extra oxygen atoms it is likely that they are distributed at random on interstitial sites, for example the extra perovskite sites. On the other hand, in the fully unloaded state, $\delta$ is 0.1 (Ref. 1) and the presence of about 0.05 oxygen vacancies per Bi atom is expected with respect to the optimal stoichiometry. Even in this case a random distribution of these defects, possibly on the pseudoperovskite sites, could explain the unchanged structural features.

To sum up, during oxygen un- and overloading the stoichiometry changes by adjusting the occupancy of the pseudoperovskite sites and possibly by inserting a few interstitial oxygen atoms between them, without any effect on the period of the modulation and on the HREM contrast.

### F. Iodine intercalation

The behavior of Bi-2212 and $Bi_{10}Sr_{15}Fe_{10}O_{46}$ is no longer similar from the point of view of iodine intercalation. In fact, the intercalation does not take place with the Fe compound, at least under conditions in which the cuprate is readily intercalated. In the host Bi-2212 structure, iodine is present as tri-iodide ion chains between the pairs of BiO layers.[35] The only structural explanation of this difference between the two compounds is the different average distance between neighboring BiO layers. In the $Bi_{10}Sr_{15}Fe_{10}O_{46}$ crystal the maximum BiO-BiO distance is 0.26 nm, whereas it is more than 0.3 nm in the cuprate. Considering that the $c$ parameter of the Fe compound is longer than that of Bi-2212, this seems to indicate that the perovskite blocks of the cuprate are more compact and the BiO layers more weakly bound than in $Bi_{10}Sr_{15}Fe_{10}O_{46}$.

### G. Structure and structural disorder of $Bi_2Sr_2Ca_{1-y}Y_yCu_2O_{8+\delta}$: The extra oxygen due to Y substitution for Ca

Both the period of the structural modulation and the $c$ parameter of the $Bi_2Sr_2Ca_{1-y}Y_yCu_2O_{8+\delta}$ single crystals are sensitive to the presence of Y, shortening with increasing Y content. Detailed characterization of these materials is reported elsewhere.[20] The period of the modulation varies from $4.76a$ in the pure Ca phase to $4.05-4.1a$ in the pure Y compound. Our [001] zone axis HREM observations show that, for low Y concentrations, the Y-substituted crystals are very similar to the pure phase materials: the contrast does not change, indicating that rocksalt and pseudoperovskite regions are still present and have the same nature [Fig. 6(a)]. Simulations using a different structural model have not shown agreement with the experimental observations.[18] In increasing the amount of Y, the number of 4- and 4.5-fold supercells increases at the expense of the fivefold ones. This is consistent with the shortening of the period of the modulation, which even in this case is related to the average distance between the extra oxygen atoms at the center of the pseudoperovskite regions in the BiO planes. Therefore the effect of the extra oxygen introduced by substituting Y for Ca, at the first stages of substitution, is the reduction of the fraction of rocksalt regions.

At high Y content, in concomitance with the metal-insulator transition,[20] the situation is completely different as shown in Fig. 6(b): the modulation is dominated by an antiphase boundary structure due to a regular shift along **b** of adjacent domains, the translation vector being (1/4)[010]. Since the spacing between antiphase boundaries is not strictly periodic, this defect does not produce extra spots on the electron-diffraction patterns, but only diffuse streaking parallel to the modulation direction. The Y distribution in our crystal is not very homogeneous.[20] For this reason we could observe, even in the weakly substituted crystals, the same kind of shift at the boundary between rocksalt and pseudoperovskite regions, possibly because of a very high local Y concentration, as shown in Fig. 6(a). The same figure shows that sometimes it is difficult to locate the columns of cations because the white dots merge in lines parallel to the $b$ axis indicating a lack of periodicity along the $c$ axis. This kind of disorder can be attributed to the coexistence along **c** of regions with the normal arrangement (low Y content) and regions which have been shifted due to an antiphase boundary (high Y content). The presence of antiphase boundaries suggests the existence of a new Bi-O arrangement able to accommodate the excess of oxygen introduced by high amounts of Y. Unfortunately, the models available, which are either based on different distributions of oxygen atoms on the perovskite sites,[18] or simply on the positional modulation of the metal atoms without considering the extra oxygen atoms,[21] do not predict the antiphase boundary structure. With increasing Y substitution the oxygen content in $Bi_2Sr_2Ca_{1-y}Y_yCu_2O_{8+\delta}$ increases, $\delta$ is 0.21 in the pure Ca phase and 0.51 in the pure Y one, and the period of the modulation decreases.[23] The proportion of perovskite to rocksalt regions increases because of the increasing number of $4a$ and $4.5a$ supercells at the expense of $5a$ ones. Beyond a certain limit however, the accommodation of extra oxygen in the BiO layers no longer occurs by reducing the extent of rocksalt regions. If this were the case the period of the modulation corresponding to the pure Y compound would be $2a$ and not $4a$. This means that a second mechanism must intervene to accommodate further amounts of oxygen with no consequence on the period of the modulation.

We suggest that the antiphase boundary structure in the highly substituted compound [Fig. 6(b)], the insulating behavior and any new means of accepting extra oxygen are all related. The deleterious effect of the translation interfaces on the electronic properties is quite obvious: they affect the geometry of the $CuO_2$ planes [Fig. 6(c)]. Figure 6(b) shows that the spacing between antiphase boundaries is 2 or $2.5a$ and this means a discontinuity every 1.52 or 1.9 nm along the Cu-O conducting path. The disappearance of superconductivity is not surprising because these distances are of the same order as the in-plane coherence length.[36]

The origin of the translation interface is not completely clear, but it is certainly related to the increasing fraction of Y atoms on the Ca sites. However, a particular ordering of Y and Ca does not seem a reasonable explanation. In fact, at the antiphase boundaries the coordination of Ca and Y atoms changes from eightfold to sixfold, which both prefer, but the coordination polyhedron is an unusual triangular prism and not a regular oxygen octahedron. This unnatural coordination appears more as a consequence of, than as a reason for, the antiphase boundary structure and suggests that the action of Y is indirect and occurs via the incorporation of extra oxygen in the BiO sheets. This indicates that further oxygen atoms inserted in the crystal, instead of occupying the available perovskite sites, reside elsewhere in the BiO layers and that the new BiO arrangement is responsible for the shift along the $b$ axis which characterizes the domain boundaries. A fact that corroborates this suggestion is the local appearance of antiphase boundaries at the interface between rocksalt and perovskite regions even in the low-substituted crystals possibly due to a local high concentration of yttrium and hence of oxygen, as shown in Fig. 6(a). We are unable to suggest a structural model based on a different Bi-O arrangement linking rocksalt and perovskite regions responsible for the antiphase boundaries for two reasons. First, high-resolution electron microscopy is not the appropriate technique for locating oxygen unambiguously because of the small scattering amplitude of oxygen with respect to the cations. Second, Bi exhibits a variety of coordinations in mixed valency bismuth oxides.[37]

## IV. CONCLUSION

High-resolution electron microscopy along the $c$ axis has been used to examine the local structural variations in the modulated $Bi_2Sr_2CaCu_2O_{8+\delta}$ and $Bi_{10}Sr_{15}Fe_{10}O_{46}$ single crystals.

In both phases the structural disorder, of which the structural modulation is one aspect, results from the labile nature of oxygen in the BiO planes. In our structural model, which has been refined by comparing observed and computed images, BiO layers consist of pseudoperovskite regions, with a fixed width, spaced by rocksalt regions of different sizes. Each perovskite region contains an extra oxygen atom at its center. The period of the modulation corresponds to the average distance between extra oxygen atoms. In the pseudoperovskite regions only three sites out of the six available are

occupied by oxygen. All the structural defects observed in both materials derive from the fact that in adjacent unit cells different kinds of sites are occupied. The different choice can take place along any axis and often involves also a variation of the size of rocksalt regions. This creates a tridimensional mosaic structure. The proposed structural model describes not only the local perfect structure of the individual domains of the $Bi_2Sr_2CaCu_2O_{8+\delta}$ and $Bi_{10}Sr_{15}Fe_{10}O_{46}$ crystals, but also all the observed defects at their boundaries.

In the Fe compound the modulation is almost commensurate: despite the disorder most of the unit cells are $5a$ wide. Therefore, it was possible to refine the average structure on the basis of a strictly commensurate model using global diffraction techniques. In contrast, the average structure of Bi-2212 is still an open question. Considering the mosaic nature of the material and the fact that often the extent of an ''ordered'' domain along the $c$ axis is half a unit cell, the concept of average structure does not seem an appropriate description of the cuprate crystal. This raises the question as to whether these local structural variations, and their associated ''impurity potential,'' contribute significantly to flux pinning. Comparisons with $Tl_2Ba_2CaCu_2O_8$ at the same doping state may help elucidate this issue. This impurity potential is evidently not sufficiently large to destroy the linear-$T$ term in the penetration depth determined for high-quality $Bi_2Sr_2CaCu_2O_{8+\delta}$ crystals.[38]

In both phases, the fraction of rocksalt and pseudoperovskite regions and the consequent period of the structural modulation is determined by an optimal composition and it is not affected by oxygen stoichiometry fluctuations, which are possibly accommodated via oxygen vacancies and interstitials in the BiO layers. In contrast the introduction of extra oxygen by substituting Y for Ca in the cuprate has a more drastic effect on the structure: at low concentrations, Y reduces the size of rocksalt regions with a consequent reduction of the period of the modulation, at high concentrations, it changes even the nature of the modulation introducing an antiphase boundary domain structure possibly related to a different kind of BiO coordination. The altered modulation is the structural signature of the superconducting-insulating transition in these compounds. The suppression of superconductivity is a consequence of the fragmentation of the crystal into domains whose size is of the same order as the in-plane coherence length.

## ACKNOWLEDGMENTS

The authors are indebted to Dr. J. L. Tallon of the New Zealand Institute for Industrial Research, Lower Hutt, for helpful discussions and encouragement. We express sincere gratitude to Professor Ph. A. Buffat, Professor P. A. Stadelmann, and Professor L. Zuppiroli of the Ecole Polytechnique Fédérale de Lausanne, for their hospitality and assistance and also to Dr. J. Aebersold for providing the noise filtering program. We acknowledge the 2212(Y) single crystals provided by Dr. L. Mihaly of the SUNY at Stony Brook, New York.

## APPENDIX: PROCESSING OF HREM IMAGES: NOISE FILTERING

The information in the experimental images of incommensurate modulated structures, such as $Bi_2Sr_2Ca_{1-y}Y_yCu_2O_{8+\delta}$ and $Bi_{10}Sr_{15}Fe_{10}O_{46}$, can be enhanced by noise filtering in Fourier space. This method takes advantage of the fact that all the information concerning a periodical structure is concentrated in the maxima of its Fourier transform, whereas the noise is randomly distributed. Despite its incommensurate nature the structural modulation produces sharp superstructure reflections in the diffraction patterns. Therefore by using a mask that selects the sharp maxima due to the basic crystal and those due to the structural modulation, and doing a second Fourier transform it is possible to reconstruct the original image without the contribution of noise. This applies even when structural defects are present because they can be considered as an isolated perturbation of the lattice.

The main drawback of the use of Fourier space processing is that an inappropriate mask can introduce artifacts. However the structural modulations and all the crystal defects studied in this work have been firstly detected on the original micrographs so that they cannot be interpreted as reconstruction artifacts.

Images with 256 gray levels and typical size of $512\times512$ pixels corresponding to areas from $8\times8$ to $14\times14$ nm in the crystals, i.e., containing from $15\times15$ to $25\times25$ basic unit cells, respectively, were digitized using a charge-coupled device TV camera and then processed with SEMPER VI software.[27] In the case of images corresponding to unfaulted regions intensity profiles have been calculated along the $a$ direction in order to correlate the modulation of the contrast to the distribution of integral domains of different sizes.

The first treatment to improve the image quality was histogram equalization, which increases the image contrast by adjusting the image pixel statistics without considering any spatial correlation present in the image. Then the Fourier transform and the corresponding power spectrum of the histogram-equalized images were calculated. Usually, at this stage, a Bragg filter, which is defined as a mask in Fourier space with circular ''holes'' at the positions of the intense Bragg reflections, is applied. In order to avoid the discontinuous edges of this kind of filter and to preserve the symmetry of the original intensity peaks, in this work soft filters based on Bragg filters with Gaussian-shaped intensity profiles were used. The same image was filtered using different threshold values and different window sizes in order to optimize the noise reduction. In order to estimate the information loss caused by filtering, the discarded image frequencies in real space were examined by applying a complementary filter to the Fourier transform of the histogram-equalized images.

Figures 7 and 8 show two examples of noise filtering on HREM images of Y-substituted Bi-2212 single crystals with low and high yttrium content, respectively, in the projection down the $c$ axis. To the eye the presence of a modulation in both experimental raw images [Figs. 7(a) and 8(a)] is obvious. The antiphase domain structure characteristic of the high yttrium content materials can also be recognized in Fig. 8(a). Histogram-equalized images extracted from the raw images are shown in Figs. 7(b) and 8(b) and indeed show some improvement in the image contrast. The corresponding power spectra (log display) are displayed in the inset. Images reconstructed by inverse transformation from the soft Gaussian and from the complementary filtered FT are shown in Figs. 7(c), 8(c), 7(d), and 8(d), respectively. The latter images mainly consist of noise.

[1] H. W. Zandbergen, W. A. Groen, F. G. Mijlhoff, G. van Tendeloo, and S. Amelinckx, Physica C **156**, 325 (1988).
[2] P. Goodman, P. Miller, T. J. White, and R. L. Withers, Acta Crystallogr. Sect. B **48**, 376 (1992).
[3] M. Terauchi and M. Tanaka, Acta Crystallogr. Sect. A **49**, 722 (1993).
[4] G. Calestani, C. Rizzoli, M. G. Francesconi, and G. D. Andretti, Physica C **161**, 598 (1989).
[5] A. I. Beskrovnyi, M. Dlouha, Z. Jirak, S. Vratislav, and E. Pollert, Physica C **166**, 79 (1990).
[6] A. I. Beskrovnyi, M. Dlouha, Z. Jirak, and S. Vratislav, Physica C **171**, 19 (1990).
[7] A. A. Levin, Yu I. Smolin, and Yu F. Shepelev, J. Phys. Condens. Matter **6**, 3539 (1994).
[8] H. Budin, O. Eibl, P. Pongratz, and P. Skalicky, Physica C **207**, 208 (1993).
[9] W.-B. Wu, L.-B. Wang, J.-S. Zhu, X.-G. Li, G.-E. Zhou, Y.-T. Qian, Z.-Y. Chen, and Y.-H. Zhang, J. Appl. Phys. **76**, 2924 (1994).
[10] X. B. Kan and S. C. Moss, Acta Crystallogr. Sect. B **48**, 122 (1992).
[11] N. D. Zhigadlo, J. Phys. Condens. Matter **6**, 8969 (1994).
[12] R. E. Gladyshevskii and R. Flukiger, Acta Crystallogr. Sect. B **52**, 38 (1996).
[13] V. Patricek, Y. Gao, P. Lee, and P. Coppens, Phys. Rev. B **42**, 387 (1990).
[14] A. Yamamoto, M. Onoda, E. Takayama-Muromachi, F. Izumi, T. Ishigaki, and H. Asano, Phys. Rev. B **42**, 4228 (1990).
[15] E. A. Hewat, J. J. Capponi, and M. Marezio, Physica C **157**, 502 (1989).
[16] T. Onozuka, T. Kajitani, M. Hirabayashi, H. Sato, and T. E. Mitchell, Jpn. J. Appl. Phys. **28**, L1775 (1989).
[17] C. C. Torardi, J. B. Parise, M. A. Subramanian, J. Gopalakrishnan, and A. W. Sleight, Physica C **157**, 115 (1989).
[18] A. I. Beskrovnyi, Z. Jirak, M. Nevriva, and I. G. Shelkova, Physica C **206**, 27 (1993).
[19] S. Kambe, K. Okuyama, S. Ohshima, and T. Shimida, Physica C **250**, 50 (1995).
[20] C. Kendziora, L. Forro, D. Mandrus, J. Hartge, P. Stephens, L. Mihaly, R. Reeder, D. Moecher, M. Rivers, and S. Sutton, Phys. Rev. B **45**, 13 025 (1992).
[21] T. Onozuka, Y. Iwabuchi, T. Fukase, H. Sato, and T. E. Mitchell, Phys. Rev. B **43**, 13 066 (1991).
[22] J. G. Wen, Y. F. Yan, and K. K. Fung, Phys. Rev. B **45**, 12 561 (1992).
[23] D. B. Mitzi, L. W. Lombardo, A. Kapitulnik, S. S. Ladermann, and R. D. Jacowitz, Phys. Rev. B **41**, 6564 (1990).
[24] Y. Le Page, W. R. McKinnon, J.-M. Tarascon, and P. Barboux, Phys. Rev. B **40**, 6810 (1989).
[25] N. Motohira, K. Kuwahara, T. Hasegawa, K. Kishio, and K. Kitazawa, J. Ceram. Soc. Jpn. Int. ed. **97**, 994 (1989).
[26] P. A. Stadelmann, Ultramicroscopy **21**, 131 (1987).
[27] W. O. Saxton and T. J. Pitt, Ultramicroscopy **4**, 343 (1979).
[28] R. de Ridder, J. van Landuyt, and S. Amelinckx, Phys. Status Solidi A **9**, 551 (1972).
[29] G. van Tendeloo and S. Amelinckx, Phys. Status Solidi A **43**, 553 (1977).
[30] J. van Landuyt, R. de Ridder, R. Gevers, and S. Amelinckx, Mater. Res. Bull. **5**, 353 (1970).
[31] Y. Matsui, H. Maeda, Y. Tanaka, S. Horiuchi, S. Takekawa, E. Takayama-Muromachi, A. Umezono, and K. Ibe, Jeol News **26** E, 36 (1988).
[32] J. M. Tarascon, P. F. Miceli, P. Barboux, D. M. Hwang, G. W. Hull, M. Giroud, L. H. Greene, Y. LePage, W. R. McKinnon, E. Tselepis, G. Pleizier, M. Eibschutz, D. A. Neumann, and J. J. Rhyne, Phys. Rev. B **39**, 11 587 (1989).
[33] X. B. Kan, J. Kulik, P. C. Chow, S. C. Moss, Y. F. Yan, J. H. Wang, and Z. X. Zhao, J. Mater. Res. **5**, 731 (1990).
[34] K. Fujiwara, J. Phys. Soc. Jpn. **12**, 7 (1957).
[35] T. Stoto, D. Pooke, and K. Kishio, Phys. Rev. B **51**, 16 220 (1995).
[36] A. P. Molozemoff, in *Physical Properties of High Temperature Superconductors I*, edited by D. M. Ginsberg (World Scientific, Singapore, 1989), p. 129.
[37] N. Kumada, N. Kinomura, P. M. Woodward, and A. W. Sleight, J. Solid State Chem. **116**, 281 (1995).
[38] T. Jacobs, S. Sridhar, Q. Li, G. D. Gu, and N. Koshizuka, Phys. Rev. Lett. **75**, 4516 (1995).